

Article

Vehicle Model-Based Driving Strategy Optimization for Lightweight Vehicle

Zoltán Pusztai , Péter Kőrös , Ferenc Szauter and Ferenc Friedler 

Vehicle Industry Research Center, Széchenyi István University, Egyetem tér 1, H-9026 Győr, Hungary; korosp@ga.sze.hu (P.K.); szauter@ga.sze.hu (F.S.); f.friedler@ga.sze.hu (F.F.)

* Correspondence: pusztai.zoltan@ga.sze.hu

Abstract: In this paper, driving strategy optimization for a track is proposed for an energy efficient battery electric vehicle dedicated to the Shell Eco-marathon. A measurement-based mathematical vehicle model was developed to simulate the behavior of the vehicle. The model contains complicated elements such as the vehicle's cornering resistance and the efficiency field of the entire powertrain. The validation of the model was presented by using the collected telemetry data from the 2019 Shell Eco-marathon competition in London (UK). The evaluation of applicable powertrains was carried out before the driving strategy optimization. The optimal acceleration curve for each investigated powertrain was defined. Using the proper powertrain is a crucial part of energy efficiency, as the drive has the most significant energy demand among all components. Two tracks with different characteristics were analyzed to show the efficiency of the proposed optimization method. The optimization results are compared to the reference method from the literature. The results of this study provide an applicable vehicle modelling methodology with efficient optimization framework, which demonstrates 5.5% improvement in energy consumption compared to the reference optimization theory.

Keywords: energy efficiency; optimization; driving strategy; powertrain; Shell Eco-marathon; electric vehicles



Citation: Pusztai, Z.; Kőrös, P.; Szauter, F.; Friedler, F. Vehicle Model-Based Driving Strategy Optimization for Lightweight Vehicle. *Energies* **2022**, *15*, 3631. <https://doi.org/10.3390/en15103631>

Academic Editor: Tek Tjing Lie

Received: 7 April 2022

Accepted: 11 May 2022

Published: 16 May 2022

Publisher's Note: MDPI stays neutral with regard to jurisdictional claims in published maps and institutional affiliations.



Copyright: © 2022 by the authors. Licensee MDPI, Basel, Switzerland. This article is an open access article distributed under the terms and conditions of the Creative Commons Attribution (CC BY) license (<https://creativecommons.org/licenses/by/4.0/>).

1. Introduction

Nowadays, the popularity of electric vehicles (EVs) is constantly increasing, even as improving the energy diversification in transportation and the potential CO₂ reduction of EVs is underestimated [1,2]. It is now technically feasible to convert 72.3 percent of the transportation demand from fossil fuels to electricity. The total energy demand might be reduced by 50.6 percent due to this approach and the improved energy efficiency of electrically powered vehicles [3]. Alternative powertrains and the use of lightweight materials are two more possible options for lowering energy consumption and CO₂ emissions [4]. Lightweight electric vehicles (LEVs) are intriguing because they combine the benefits of both EVs and lightweight vehicles. A reduced weight improves the range of an electric vehicle, which is still a major concern. This effect can be strengthened even further by weight loss [5]. The environmental impact of cars makes up the largest share of the total global impact of passenger transport. EU directives set in 2015–2020 are putting pressure on the car industry to meet CO₂ emission targets, with potentially significant economic and financial consequences [6].

Intensive research efforts aiming at improving vehicle energy efficiency are linked to the transition from fossil-fuel-based transportation to electric mobility. The Shell Eco-marathon is an annual international engineering competition for student teams. The competition serves as a platform for innovative approaches to creating fuel-efficient automobiles. The goal of the Mileage Challenge is to complete a valid race in the shortest length of time while consuming the least amount of electric energy or fuel. Vehicles must cover roughly 16 km in under 40 min. Vehicles are divided into three categories based

on their architecture (Prototype and Urban Concept (UC)) and energy consumption (internal combustion engine vehicles, battery electric vehicles (BEVs), and hydrogen fuel cell vehicles). The three-wheeled prototype vehicles have extremely low aerodynamic drag. The urban concept vehicles must make a full stop after each lap, unlike prototype vehicles. The goal of the UC category is to simulate urban transportation, which includes slow speeds and frequent stops. The Shell Eco-marathon is the most prestigious energy efficiency race, which has been held in Europe since 1985, with more than 200 teams from renowned European technical universities participating in the 2017 edition. Several world records in fuel efficiency have been set by specifically equipped automobiles during the SEM series [7].

The current vehicle development mainly focuses on the electric and mechanic energy loss reduction in the powertrain, rolling elements (suspension and steering system), and system electronics. The development of the physical components of the vehicle is inadequate to reach the desired overall vehicle efficiency without proper vehicle operation because the driver has general impact on the energy utilization [8]. Eco-driving can be achieved by applying optimal driving strategy. The optimal driving strategy is determined by the corresponding velocity profile to the given track. The velocity profile can be obtained by solving an optimal control problem, where the optimization objective is the minimization of energy usage [9]. Several SEM-specific model-based approaches of driving strategy optimization can be found in the literature; research mainly focuses on prototype vehicles.

Model-based optimization was performed on an electric prototype vehicle in Ref. [10], where the model was built based on experimental results. The powertrain efficiency maps and coast-down test results were used in the simulation model. The cornering losses were neglected in the created vehicle model, but the effect of cornering was implemented in velocity strategies where speed limitations were made in cornering. The track was divided into segments to consider the optimization. The optimization was carried out with the Genetic Algorithm (GA) and the result was 30% better (including driving errors) than the driving strategy of the human driver [10].

The control strategy of an internal combustion engine powered prototype vehicle is investigated in Ref. [11], where evolutionary optimization methods were compared. The results have shown that the most promising results are obtained by the Jaya (JA) algorithm; approaches of Particle Swarm Optimization (PSO) and Grey Wolf Optimizer (GWO) produced significantly faster results than other methods. The optimization outcomes of Firefly (FA) and Invasive Weed Optimization (IWO) methods were not comparable. The research also demonstrated the inefficiency of the traditional gradient-based optimization strategies such as Sequential Quadratic Programming (SQP). The inertia of rotational parts was neglected [11].

The multi-physics model of a hydrogen powered UC vehicle was proposed in Ref. [12], highlighting the modelling of power converter, fuel cell, and ironless motor. The vehicle model is not based on measurements and the resistance of cornering is neglected. The power losses of each subcomponent are presented in detail. A PSO algorithm was used in the optimization process, where the motor currents, maximum and minimum speeds, and gearbox ratio was optimized [12]. Fuel cell vehicle was also modelled and optimized in Ref. [13] with a complete powertrain model, but the cornering resistance was also neglected.

The design process and the vehicle simulation of a battery electric UC vehicle were described in Ref. [14]. The vehicle model was built combining theoretical calculations and measurements. The powertrain model is measurement-based, but the resistance forces are calculated with vehicle and track constants. The resistance of cornering is implemented in the vehicle model. Sensitivity analysis of energy consumption of an SEM vehicle was performed on three different tracks in Ref. [15]. The vehicle mass reduction provides the highest benefits in energy savings; 10% mass reduction leads to 5.5% to 8% energy savings, depending on the track. The aggressiveness parameter of the track was also considered in the simulation, and the contribution of cornering losses was stated as a non-negligible factor with 5% to 12% power loss, depending on track [15].

The literature includes several mathematical optimization methods to define the optimal velocity profile for a track. In case of different compatible powertrains, the optimal velocity profile is different for each track. The cornering radius should not be neglected and should be properly attached to the track profile. The measurement-based models could have included the effect of cornering [16] and a new approach of optimization methodology is proposed.

Hybrid driving strategy optimization was proposed in Ref. [17], where the driving strategy and the optimization process was supported by cognitive infocommunications. The genetic algorithm-based optimization is supported by human driving experience, considering the instincts of the driver. The human driven laps are provide the initial input for the optimization, which significantly improves the optimization time and results.

2. Vehicle Design

SZEnergy Team is the student team of Széchenyi István University, located in Győr, Hungary. The team has been participating in the SEM series since 2005. At first, solar cell powered electric cars were built which brought lots of success to the team, winning the category several times. Then, an energy category change was made, and since 2013 the team have been developing battery electric vehicles. The first battery electric vehicle created, called SZElectricity, achieved third place in two consecutive years, 2015 and 2016. The team's actual racing vehicle, called SZEmission, was showcased in 2019 and achieved sixth place in the most recent on-track event of SEM in 2019, London. In the past years, no physical SEM event took place due to the restrictions of the COVID-19 pandemic.

SZElectricity (Figure 1a) was introduced in 2013, specially designed according to the race regulations of SEM. The chassis of the one-seated battery electric vehicle was made of carbon composite, but the vehicle body was a welded aluminum frame. The vehicle was equipped with purpose-made power electronics and a telemetry system. The body shape of the chassis was not investigated in simulation environment at that time, therefore the vehicle had considerable losses from aerodynamic drag.



Figure 1. Investigated Urban Concept SEM vehicles: (a) SZElectricity; (b) SZEmission.

After 5 years, the SZElectricity (Figure 1a) had reached its peak; in addition, a new regulation modification in the UC category required two passenger doors from 2019. This marked the beginning of the development process of SZEmission in 2018.

The main goal was to design and build a competitive vehicle with carbon monocoque chassis and low aerodynamic drag, correcting the main drawbacks of the previous structure. The whole vehicle body was made from carbon fiber reinforced polymer composite with paper honeycomb structure. This structure guarantees extreme rigidity at relatively low weight. The suspension system was designed to be able to carry different powertrains for test reasons. The system electronics were also improved while keeping the sinusoidal three phase motor controller from the previous vehicle. The vehicle control unit (VCU) is responsible for the drive and all peripheries of the vehicle. The vehicle is able to participate in autonomous SEM events too, as the vehicle body and system electrics were designed

to participate in Autonomous SEM events as well as the Mileage Challenge. The main differences in the vehicle parameters are shown in Table 1. SZEmission is going to be under the scope of the current study, using SZElectricity as a reference vehicle.

Table 1. Vehicle parameters.

Parameter	SZElectricity	SZEmission
Vehicle frame	Tubular Aluminum	Carbon Monocoque
Powertrain	PMSM direct drive	PMSM/BLDC with belt drive
Drag coefficient	0.34	0.1
Vehicle mass (without driver)	101 kg	93 kg

3. Mathematical Vehicle Modelling

In the literature of energy efficient lightweight vehicles, two modelling approaches can be found. The equation-based modelling uses descriptive theoretical equations with variables that can be conducted from simulations and measurements. The accuracy of the model can be improved by in depth investigation of subassemblies, similar to Ref. [12], where the multiphysics modelling approach was expanded to the level of fuel cells. The disadvantage of this method is that it relies on simplification to some extent. A kinematic bicycle model was used to determine eco-driving strategy, including the cornering effect for electric vehicles in urban scenarios in Ref. [18]. The other way to describe the characteristics of the examined vehicle is the measurement-based vehicle modelling [16], which is a grey box modelling approach. Systematic measurements were set up to describe the important subassemblies of the vehicle. The model can be used to solve the optimization of ecodriving problems for energy efficient lightweight vehicles. The proposed model describes the complete powertrain, vehicle dynamics, and resistance and contains the characteristics of the entire track, including the impacts of cornering. The schematics of the proposed and developed vehicle model can be seen in Figure 2.

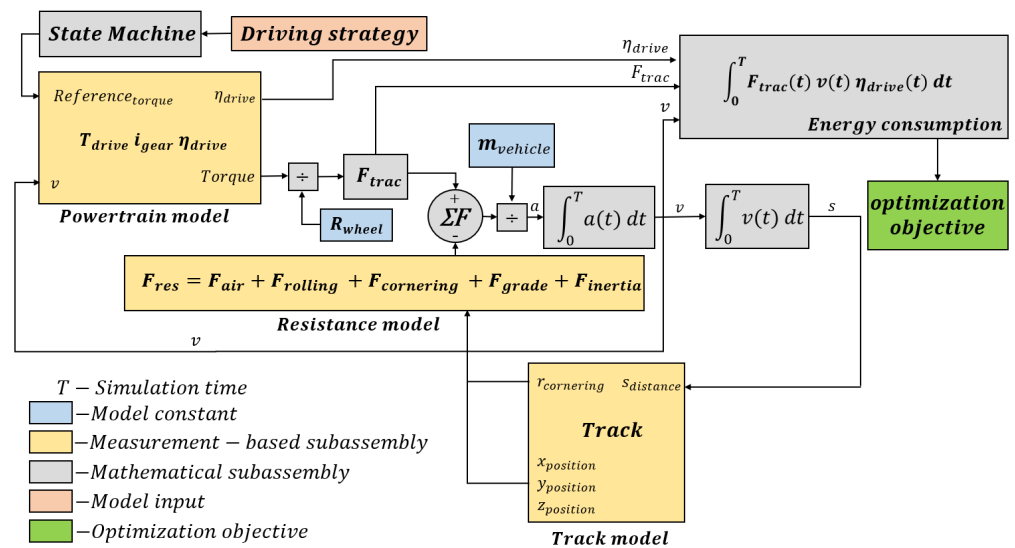


Figure 2. Overview of the vehicle model [16].

The mathematic background of the vehicle model needs to be set up. The longitudinal vehicle dynamics are described according to Equation (1).

$$ma(t) = F_{trac}(t) - F_{res}(t) \tag{1}$$

where m and a denote the vehicle’s overall mass (including the driver) and acceleration, respectively. The total traction force F_{trac} , generated by the powertrain, accelerates the

vehicle against the cumulative resistance forces F_{res} . The traction force is defined in Equation (2).

$$F_{trac} = \frac{T_{drive} i_{gear} \eta_{drive}}{R_{wheel}} \quad (2)$$

where T_{drive} is the generated torque by the electric motor, i_{gear} is the gear ratio of the synchronous belt connection, and η_{drive} is the measured efficiency of all drive components. The numerator contains the effective torque of the drive, divided by the wheel radius R_{wheel} . The resistance forces can be calculated using Equation (3).

$$F_{res} = F_{air} + F_{rolling} + F_{cornering} + F_{grade} + F_{inertia} \quad (3)$$

The decreasing of air resistance F_{air} and rolling resistance $F_{rolling}$ are the main development directions of an energy efficient vehicle, besides decreasing the mass of the vehicle which correlates to the $F_{inertia}$. The cornering resistance $F_{cornering}$ is a surplus rolling resistance arising during cornering, which should not be neglected. The resistance coming from the elevation of the track is called grade resistance F_{grade} and, with $F_{cornering}$, these are track related components.

The main advantage of a measurement-based modelling approach is to include all the described equations in dedicated model subassemblies. The suggested vehicle model has three major subassemblies that can be identified using laboratory tests and field measurements. The model was elaborated in a MATLAB and Simulink environment.

3.1. Powertrain Model

The vehicle can be driven by several types of permanent magnet synchronous machines (PMSM) and brushless DC (BLDC) motors with a purpose-made motor controller. In all powertrain designs, the electric motor drives the rear left wheel, either through synchronous belt connection or directly. The belt connection provides a further opportunity to refine the drive configuration, as gear ratios can be applied up to 4. The proposed powertrain model is suitable to include the effect of all drive elements (PMSM/BLDC-controller-transmission). In this study, four different types of drive were investigated (Table 2), which are all feasible in SEM vehicles.

Table 2. The properties of the applicable powertrains.

Powertrain	QB3403	SZEVOL	Volcano	Emoteq
Type	PMSM	BLDC	BLDC	PMSM
Sensor	Encoder + Hall	Hall	Hall	Encoder + Hall
Voltage	48 V	48 V	48 V	48 V
Mass	4 kg	7 kg	12 kg	14 kg
Max Torque	26 Nm	38 Nm	38 Nm	20 Nm
Max Speed	510 rpm	340 rpm	340 rpm	310 rpm
Applied Gear	4	3.6	3.6	direct

QB3403 (Figure 3a) is a NEMA 34 housed servo motor, and Emoteq (Figure 3d) is a frameless motor with custom machined housing. Volcano (Figure 3c) is also a NEMA 34 housed commercially available motor, while SZEVOL (Figure 3b) is a custom-built motor based on the structure of Volcano with mass optimized housing. An important goal is to reduce the vehicle idle electric consumption to below 1W; therefore, BLDC application is more suitable, because PMSMs are controlled by a higher energy demand encoder. All the drives are equipped with a synchronous belt connection; only the Emoteq is directly connected to the wheel, due to its physical size.

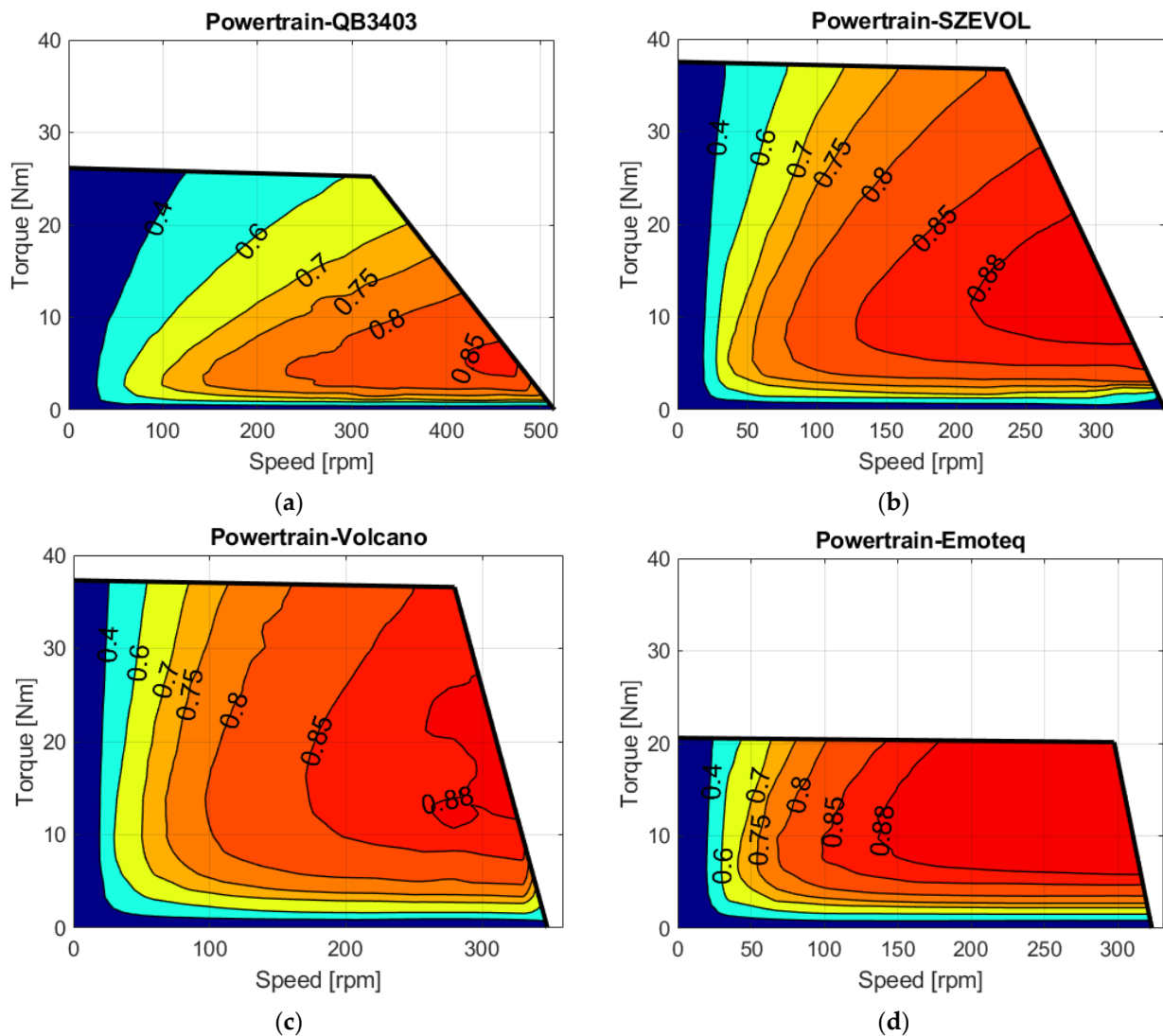


Figure 3. The measured efficiency map of the investigated powertrain, including the efficiency of the controller and transmission: (a) QB3403-PMSM; (b) SZEVOL-BLDC; (c) Volcano-BLDC; and (d) Emoteq-PMSM.

The measurements were made in an electric motor test bed laboratory dedicated for drives with a maximum power of 5 kW. This environment provides reliable accuracy. The maximum efficiency of powertrains is from 85% to 90%, but the shape of the curves is different. It is interesting to note that the maximum efficiency of Hall controlled motors is not under Encoder controlled ones; their application is also appropriate in energy efficient drives. The combined efficiency map of the powertrain was created by measuring the used electric power and the produced mechanic power according to Equation (4). The measurement is carried out automatically by the test bench environment.

$$\eta_{\text{drive}} = \frac{\int_0^t M(t)\omega(t)dt}{\int_0^t U(t)I(t)dt} \quad (4)$$

3.2. Resistance Model

The resistance model includes all factors and forces, which affects the motion of the vehicle. The classical resistance force models neglect the cornering resistance and only include the resistance factors of straight moving. The cornering resistance should not be neglected in urban vehicles, although it is complex task to determine the accurate losses.

The active frontal area and the air drag coefficient of the vehicle are changing during cornering, which affects the actual drag F_{air} . The rolling resistance is also changing during cornering due to the losses of steering elements and tires. The combined effect of these changes cannot be modelled with reasonable accuracy.

The proposed measurement-based resistance model is created by combining the resistance force in straight moving and in cornering. Two main measurement scenarios were made to determine the losses:

- Coast down test;
- Speed-controlled cornering test.

The coast down test is suitable for evaluating the acting resistance forces on the vehicle in straight motion. In the presented case, the vehicle was accelerated to the maximum speed, which depends on the gear ratio of the powertrain (40 km/h in this study), and the velocity profile of the deceleration was recorded. Coast down tests were performed two times in a row in both directions and averaged to eliminate the slope of the track and uncertain environmental conditions.

The speed-controlled cornering test was specially designed to measure the cornering losses and to complete the results of the coast down test. The cornering measurement needs a properly asphalted flat track; in the presented case, the Dynamic Platform of ZalaZone Proving Ground was used. During the test, the driver manually followed the predetermined path, while the vehicle speed was controlled by a real-time linear speed controller (PI). The motor torque and the traction force were calculated from the logged telemetry data using the previously presented powertrain model. The cornering resistance force is balanced by the traction force when the system is steady. The measured resistance force can be assigned to discrete cornering radius–vehicle speed data pairs. Turn direction sensitivity was assumed based on the unique vehicle structure and unsymmetrically placed drive, therefore all cornering measurements were made both clockwise and anti-clockwise. The inspected test scenarios are summarized in Table 3.

Table 3. Measured points of speed-controlled cornering test.

Cornering Radius	Speed
8 m	5–10 km/h
20 m	5–10–15–20–25 km/h
40 m	5–10–15–20–25–30 km/h
50 m	5–10–15–20–25–30 km/h
100 m	5–10–15–20–25–30 km/h

The evaluation of cornering tests is completed manually by matching the appropriate data pairs. The recorded traction force is sinusoidal, caused by the combined effect of the slope of the track and the low energy demand of the vehicle. The baseline of the sine needs to be found and the corresponding speed and traction force values are used for the evaluation. All test scenarios were made with the tire pressure of 5 bar, which is the usual value for SEM vehicles. An example of the speed-controlled cornering test evaluation is visualized in Figure 4.

In the coast down test, all resistance force values can be determined for every speed value, while in the cornering test, only the resistance of measured points can be assigned. A three-dimensional resistance force model can be set up, containing the following dimensions: cornering radius–speed–resistance force. The surface is created by linear interpolation between the measured data, and this interpolated surface is used in the vehicle model. The fifth grade polynomial is acquired from the coast down test and limits the surface in the cornering radius value of -200 m to 200 m. The vehicle motion is considered to be straight from the cornering radius value of $-/+200$ m. The physically reachable cornering radius value is 6 m, according to the SEM regulations [7].

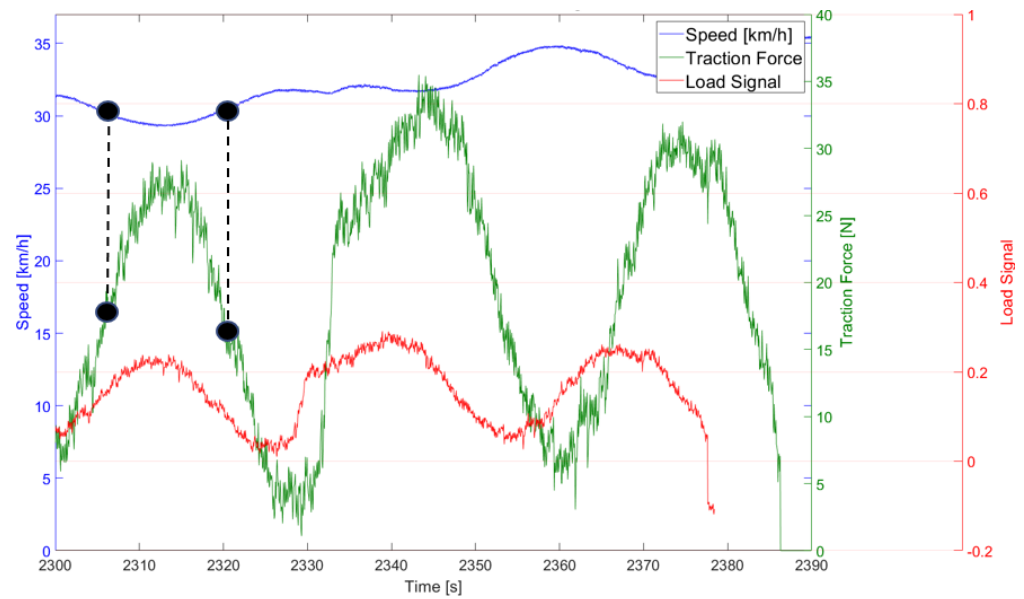


Figure 4. Example for manual cornering resistance evaluation.

The resistance model for SZElectricity (Figure 5a) and SZEmission (Figure 5b) was created from the measured data. The most significant difference can be noticed in the form the polynomial, which corresponds to the straight moving resistance. The largest improvement was achieved in the chassis, therefore the air drag is significantly lower; based on the measurement, the drag coefficient C_x value is approximately 0.1.

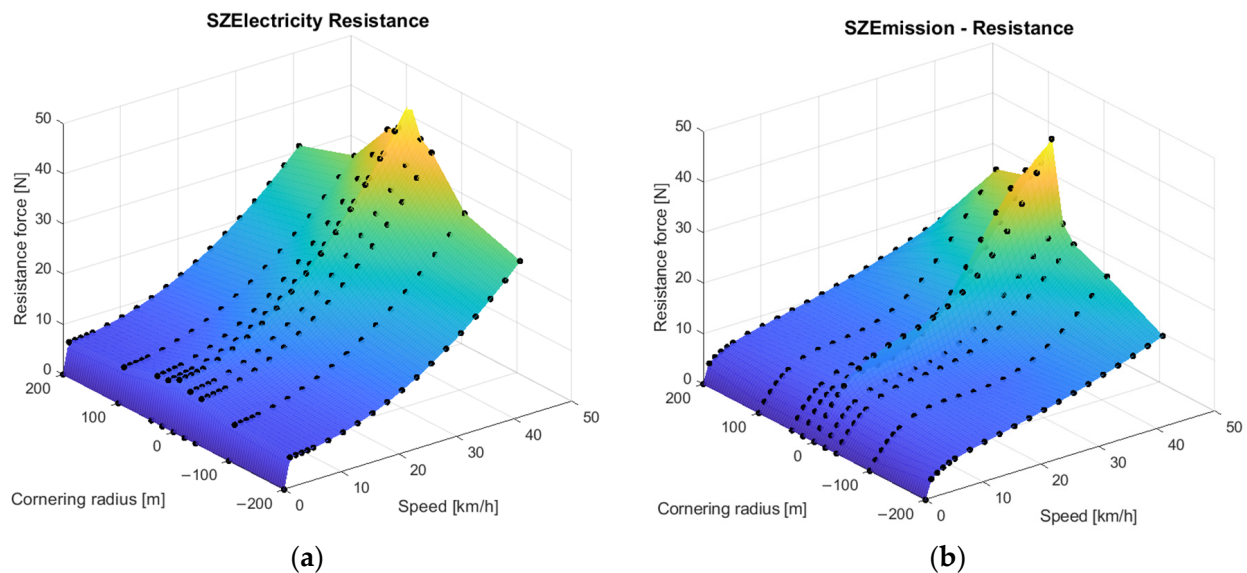


Figure 5. Three-dimensional resistance force model; (a) SZElectricity; (b) SZEmission.

3.3. Track Model

The proposed resistance model is interacting with the track model, which describes the actual parameters of the track. The track model provides input for the resistance model to calculate the track related losses, such as cornering resistance and grade resistance. The track model can be determined using the geographical coordinates of the planned route. The elevation of the track is directly determined by the z coordinates, while the cornering radius should be calculated by fitting curves to the corresponding x–y coordinates. In this study, two tracks were analyzed: the track of SEM 2019 in London (Figure 6a,c), and the Uni

Track in ZalaZone Proving Ground (Figure 6b,d). The elevation–distance and cornering radius distance data pairs describes the track characteristics.

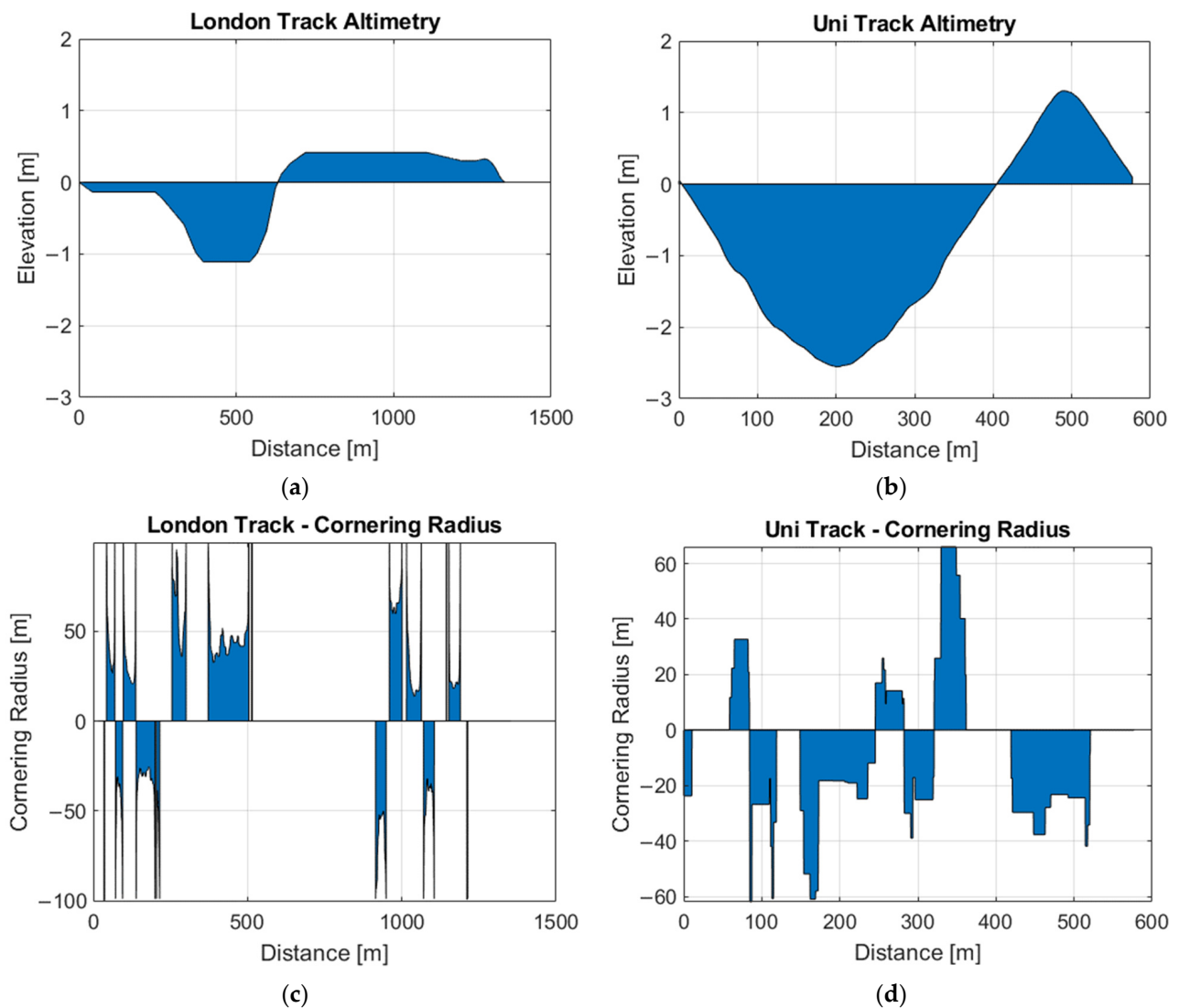


Figure 6. Properties of the investigated track; (a) elevation of London Track; (b) elevation of Uni Track; (c) cornering radius of London Track; and (d) cornering radius of Uni Track.

The creation of the London Track model was made in 2019 using publicly available geographical data, while the Uni Track was measured during the field tests. High precision GNSS (Swift Navigation-Piksi Multi GNSS) system was installed to the vehicle while it was on the track. This method gives the highest degree of precision with configurable resolution. The onboard GNSS measurement system can be also used during SEM event, determining the track model on-site. A MATLAB script was created to generate the track model based on the recorded GPS coordinates. The created model stores the track data (distance, elevation, and cornering radius) in look-up table form in the Simulink environment. The track related resistance force components (F_{grade} and $F_{\text{cornering}}$) are calculated from the track data and the actual position and vehicle speed.

4. Vehicle Model Validation and Preliminary Powertrain Evaluation

The vehicle model needs to be validated before using it for optimization purposes. The validation of the developed vehicle model was performed based on the telemetry data collected in the 2019 SEM event in London. Vehicle data are transferred with CAN communication to the vehicle control unit (VCU) measuring 96 parameters at a frequency of 20 Hz. For the validation, the measured powertrain energy usage is compared to the simulation energy usage, the minimization of which is the goal of the optimization. The velocity profile of the vehicle is determined by the motor rotational speed. The vehicle telemetry system recorded the applied load signal of the motor controller. The torque reference value can be calculated based on the applied load signal and the motor speed. The torque reference was used in the vehicle model to replay the investigated race laps. The comparison of the velocity profiles of the simulation and telemetry system data can be seen in Figure 7.

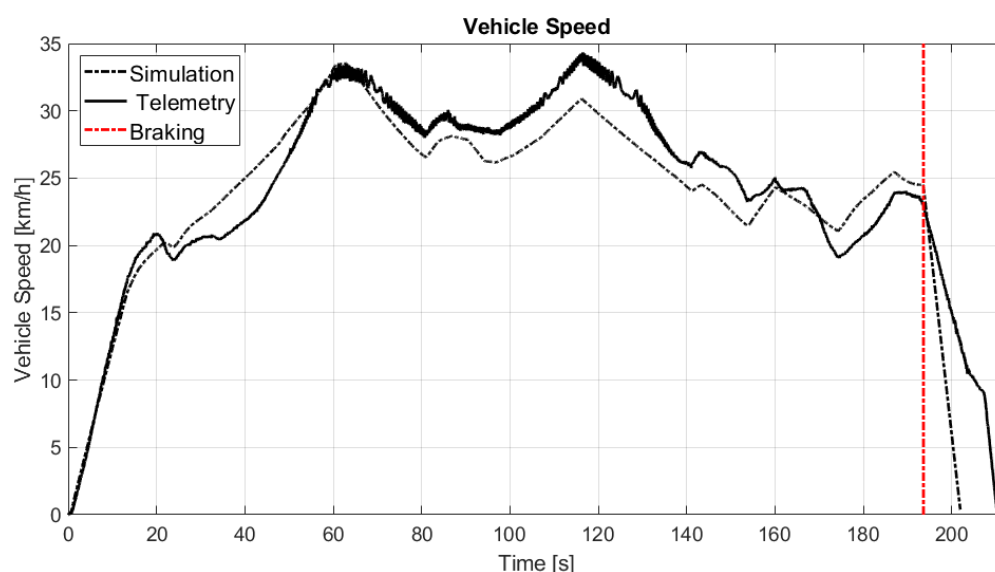


Figure 7. Comparison the simulated and recorded vehicle speed for model validation.

Solid consistency is shown by the acquired simulation velocity profile and the recorded data. The simulation is not considering the external environmental effects (wind) and the regenerative braking progress, the timing of which is highlighted by the red line. The effect of wind is clearly visible in Figure 7; the simulation vehicle speed is overshoot in the first stage of the lap (until 65 s) due to headwind. After the hairpin turn, the wind direction changed to tailwind (until 120 s) and the simulation speed is lower than the measured speed. Based on these results, the dynamic behavior of the vehicle is well described by the model. The energy consumption of the model compared to the telemetry is shown in Figure 8. The recuperated energy from regenerative braking is not calculated by the model; the braking is realized to be accomplished by constant deceleration. The result shows a 1.56% difference between the simulated and recorded energy consumption, which makes the model eligible for optimization purposes.

The energy difference was shown by the validation between the simulated and recorded data, which was mainly caused by the wind. The vehicle model includes the cornering resistance and all energy losses of the powertrain; the measurement scenarios enable us to model these complex relations more accurately without making simplifications.

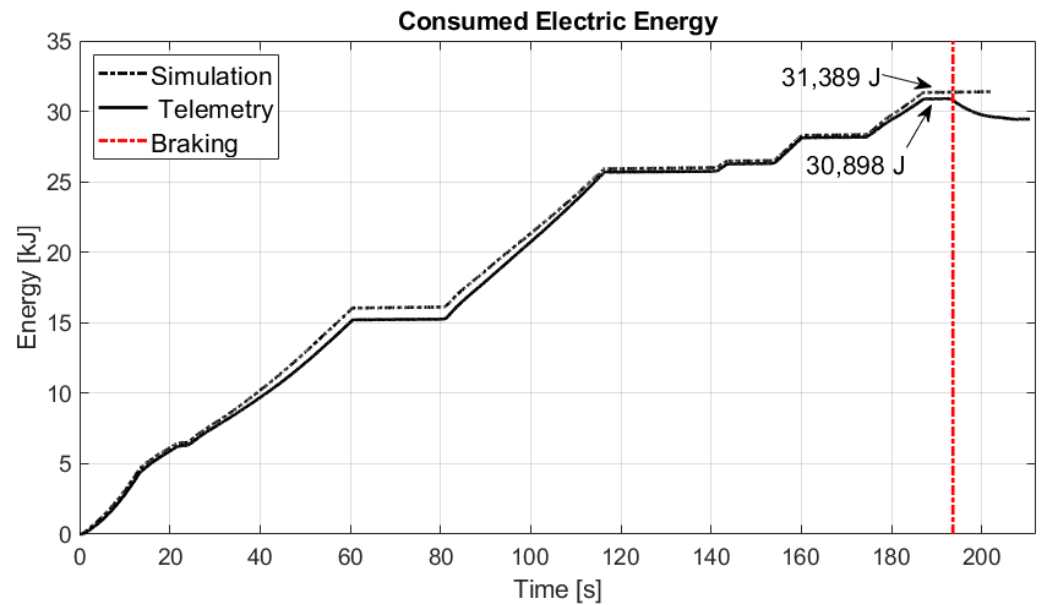


Figure 8. Comparison the simulated and recorded energy consumption for model validation.

The validated vehicle model was used for various optimization cases. A classical genetic algorithm from the Matlab Optimization Toolbox was used for the optimization. The vehicle model was implemented in Simulink, the genetic algorithm (GA) uses the model in every iteration, and the fitness function evaluates the outputs of the model. To solve optimization problems, nondeterministic processes such as selection, mutation, and crossover are applied to generate a population of candidate solutions. The solution of GA is majorly dependent on optimization settings and the characteristics of the initial population; the optimization result should not be considered a global optimum. More attempts with different randomized initial populations were made to overcome the issue of getting trapped in local minima. The application of GA in driving strategy related tasks is favorable due to its ability to solve hard, nonlinear, grey-box type problems [19,20].

The first optimization problem was formed to evaluate the applicable powertrains for the investigated vehicle. The minimization of consumed electric energy (E) is the objective function. The consumed energy is calculated according to Equation (5). The traction force $F_{\text{trac}}(t)$ is used for energy calculation and can be defined as in Equation (6).

$$\text{Minimize : } E = \int_0^T F_{\text{trac}}(t) v(t) \eta_{\text{drive}}(t) dt \quad (5)$$

$$F_{\text{trac}}(t) = \frac{M(t)}{r_{\text{wheel}}} \quad (6)$$

There was no optimization constraint formed in relation with the track, which was assumed flat, and the vehicle path was straight. In the optimization process, $N_{\text{var}} = 13$ variables were created for discrete speed values in the v vector in Equation (7), defined with the rule of Equation (8). The M optimization vector (Equation (9)) to the corresponding speed values needed to be calculated. The genetic algorithm was applied with the constraints described in Equations (10) and (11). M_{max} is the maximal applicable torque for the powertrains according to Table 2.

$$v = (v_0, v_1, \dots, v_{n-1}) \quad (7)$$

$$v_i = i \cdot 2.5 (i = 0, 1, \dots, n-1) \quad (8)$$

$$M = (M_0, M_1, \dots, M_{n-1}) \quad (9)$$

$$M_i \in \mathbb{R}^+ (i = 0, 1 \dots n) \quad (10)$$

$$0 \leq M_i \leq M_{\max} \quad (11)$$

There were three sets of optimization attempts made for each investigated powertrain for the reference vehicle (SZElectricity) and the current vehicle (SZEmission). Third order polynomial fitting was applied to create speed continuous torque relation. The covered distance and the time of acceleration were not considered in the results. The optimized torque reference curves of the powertrains of the investigated vehicles are shown in Figure 9.

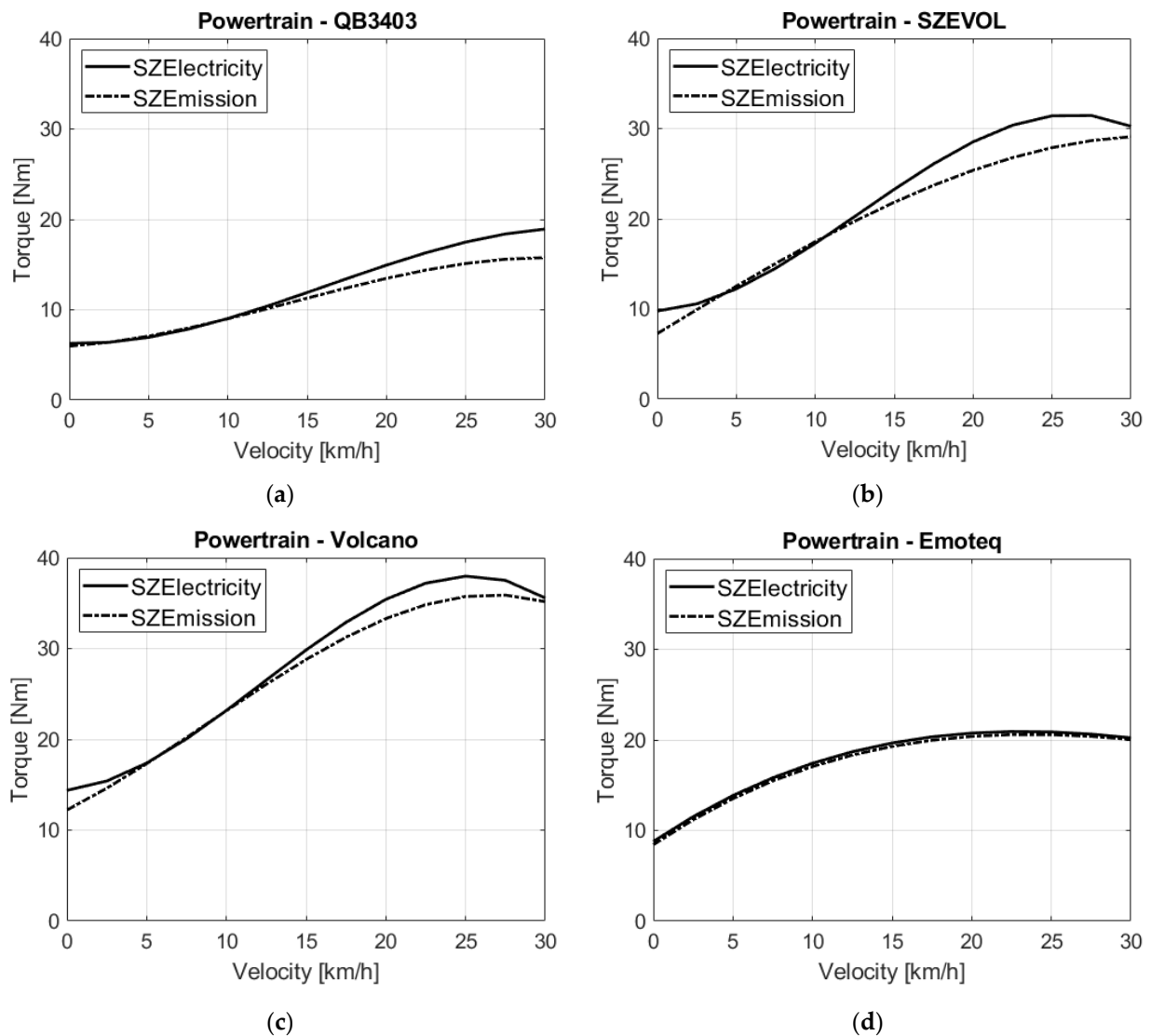


Figure 9. The optimized torque reference curves of the investigated powertrains. (a) Powertrain QB3403; (b) Powertrain SZEVOL; (c) Powertrain Volcano; and (d) Powertrain Emoteq.

From the results and the shape of the curves, the difference between the vehicles and the powertrains is clearly visible. The reference vehicle has higher power demand in every case due to its greater driving resistance, and the optimization modifies the curves respecting that. The powertrain QB3403 (Figure 9a) has low efficiency in a low speed range, making the curve flat in that area. The Emoteq powertrain (Figure 9d) is clearly undersized, as it reaches its maximum torque at low speeds. There is no apparent difference between the curves of the vehicles, which means the powertrain is the limiting factor. The torque reference curve characteristics of SZEVOL (Figure 9b) and Volcano (Figure 9c) are similar, despite the Volcano operating at higher torque values for almost the whole speed range.

The Volcano drive has less energy loss in a higher torque and speed range, therefore the optimized acceleration curve is near to the maximum available load curve. The application of the optimized acceleration curve saves a considerable amount of energy compared to the full load acceleration, but the time demand also increases. Interestingly, the form of the optimized curves does not depend on vehicle mass; they are defined by the properties of powertrain and driving resistance.

Figure 10 summarizes the consumed electric energy of each powertrain until the vehicle reaches the speed of 30 km/h, which illustrates classic SEM lap starts. Based on the results of the acceleration simulation, the Volcano powertrain was chosen for further driving strategy investigation.

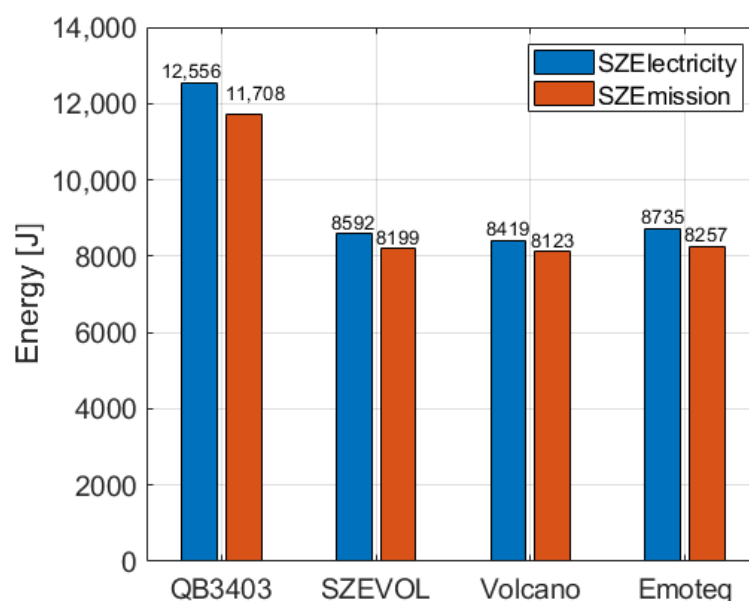


Figure 10. Consumed electric energy of the powertrains with the optimized torque reference acceleration until reaching 30 km/h.

Powertrain evaluation can be preliminary performed before starting the track optimization. The advantage of choosing the powertrain first is to save significant optimization time. The usage of the optimized acceleration curve of powertrains saves significant energy during the acceleration of the vehicle, although the time loss is not beneficial in race conditions. This result can be useful in urban vehicles in real transportation conditions, where the constraints are more relaxed and robust solution is needed, due to the disturbance of traffic.

5. Driving Strategy Optimization

The driving strategy optimization of the SZEmission vehicle was carried out to the two investigated tracks with the previously chosen Volcano powertrain. Genetic algorithm remained the optimization tool, where the fitness function was changed according to Equation (12). The goal to minimize of consumed electric energy (E) remained, even as further optimization constraints were formed.

Only one race lap is investigated with the optimization, considering the characteristics of the track and the vehicle starts from standing position. The vehicle needs to complete at least the track distance $s_{\max} - 2$ m, leaving space for the driver to maneuver correctly to the finish line, where there is usually traffic at SEM races. Due to this buffer distance, the vehicle not forced to stop; it just needs to decrease the speed below 8 km/h. The vehicle needs to finish the lap below the time limit T_{\max} . The optimization constraints are summarized in Equation (12). The actual vehicle speed is described in Equation (13).

The driving strategy optimization problem for discrete tracks can be formulated as such:

$$\text{Minimize } E \text{ subject to : } \begin{cases} s_{\max} - 2 \leq \int_0^T v(t) dt \leq s_{\max} \\ T \leq T_{\max} \\ v(0) = 0 \text{ and } v(T) \leq 8 \end{cases} \quad (12)$$

$$v(t) = \int_0^T \frac{\frac{M(t)}{r_{\text{wheel}}} - F_{\text{res}}(t)}{m_{\text{vehicle}}} dt \quad (13)$$

Description of Optimization Cases for Track Optimization

The state machine of the vehicle model was modified to adapt the proposed driving strategy in Ref. [12], which is going to be the reference optimization, as the basic principle of systematic acceleration–coast down phases is a very popular strategy in SEM events. The coasting method is also used in urban railways as a train control method to reduce energy consumption [21]. The parameter vector of that optimization method is shown in Equation (14). The gear of the powertrain remains unchanged, formulated on the results of the powertrain evaluation. The fitness function is described in Equation (12) and the parameter vector of optimization variables in Equation (14).

$$\text{opt} = \{ v_{\max}, v_{\min}, M_{\text{start}}, M_{\text{min}} \} \quad (14)$$

The main advantage of this method is the small optimization vector with only four parameters, which also means a low optimization time. The parameter constraints are described in Equation (15).

$$\text{Limits : } \begin{cases} 10 \leq v_{\max} \leq 40 \\ 1 \leq v_{\min} \leq 25 \\ 25 \leq M_{\text{start}} \leq 40 \\ 1 \leq M_{\text{min}} \leq 30 \end{cases} \quad (15)$$

The Max Torque optimization method is also based on the acceleration–coast down technique, but it has been modified to be dependent on the track, not vehicle speed. The fitness function and the optimization constraints are described according to Equations (12) and (13). Number of variable n is dependent on the track length according to Equation (16). The track distance s is divided into parts described in Equation (17), with the rule defined in Equation (18). For practical reasons, the interval of 10 m was chosen. In this optimization method, a parameter vector of z needs to be found for the corresponding s vector. The value z is defined with Equation (20). This vector provides input for the state machine which implies the torque is, in this case, maximum or zero for the determined track distances.

$$n = \frac{s_{\max}}{10} + 1 \quad (16)$$

$$s = (s_0, s_1 \dots s_{n-1}) \quad (17)$$

$$s_i = i \cdot 10 \quad (i = 0, 1 \dots n - 1) \quad (18)$$

$$z = (z_0, z_1, \dots z_{n-1}) \quad (19)$$

$$z_i = \begin{cases} 0, & \text{if } M_i = 0 \\ 1, & \text{if } M_i = M_{\max} \end{cases} \quad (20)$$

The Max Torque optimization method is suitable for finding the right track coordinates where torque should be applied by the drivetrain. The amount of applied torque is maximized to decrease possible solutions and therefore the optimization time. Previous attempts showed that if the rule in Equation (20) is not used, the genetic algorithm is not working efficiently without further assistance. The efficiency of the genetic algorithm could

be increased by adding human driven laps into the initial population (N_{pop}) such as in Ref. [17]. This method is also appropriate for choosing the right gear ratio for the actual powertrain, as the maximum torque differs of each option. The described Max Torque optimization method is mainly applied for analyzing the track and providing input for a more detailed investigation of the applied torque.

In the TRQ (Torque) optimization, the parameter vector of M is matched by the algorithm to the corresponding s vector, as described in Equation (21). TRQ optimization is carried out by using the results of the Max Torque optimization according to the rules defined in Equations (22) and (23). The rules were created to allow slight modification in timing of the torque and ensure that the parameter vector of M meets the criteria of the fitness function.

$$M = (M_0, M_1, \dots, M_{n-1}) \quad (21)$$

$$M_i \in Z^+ (i = 0, 1 \dots n - 1) \quad (22)$$

$$0 \leq M_{i \pm 1} \leq M_{max} \text{ if } z_i = 1 \\ \text{otherwise } M_i = 0 \quad (23)$$

It is essential to highlight that the Max Torque optimization must be solved first to provide input for TRQ optimization, therefore the optimization time is added. The initial population of pure TRQ optimization contains a huge number of individuals with low score of fitness when the constraint of Equation (23) is not applied. The genetic algorithm is forced to search for an appropriate value of torque for the defined track coordinates. The applicable torque values are limited to integer numbers to decrease possible solutions and the running time of optimization. In the following section, the investigated two tracks are analyzed, and driving strategy optimization methods are compared.

6. Results and Discussion

The London Track, where the last SEM event was held in 2019, was the first location to be analyzed. The track data were collected from a publicly available database. The length of the track is 1353 m, and it has slight elevation as described earlier in Figure 6. The reference optimization operates with long acceleration phases between 19 km/h and 29 km/h. The maximal vehicle speed is lower than the other two cases, which makes the third acceleration necessary. The result clearly shows the drawbacks of the few optimization variables, which cannot take the characteristics of the track into consideration. The Max Torque Optimization assigns the acceleration to the actual position to the track, not to the speed, therefore it takes advantage of the track. Regarding this method, more smaller acceleration phases can be noticed in Figure 11a. The speed peaks at almost 34 km/h, and after the last acceleration a long coast down phase starts until the end of the lap. The TRQ optimization refines the result of the previous method, mainly modifying the velocity profile between from 60 s to 100 s. The conclusion can be drawn from Figure 11b that the energy cost of the third acceleration is significant. The modification of the second acceleration phase results in the main difference between the reference and the other proposed methods.

The main parameters of the optimization for London Track are summarized in Table 4. The generation is the number of the iteration made by the genetic algorithm. The function count is the cumulative number of fitness function evaluation, and it correlates to the relation of iterations and population size [22].

The force components of the best optimization attempt for London Track is shown in Figure 12.

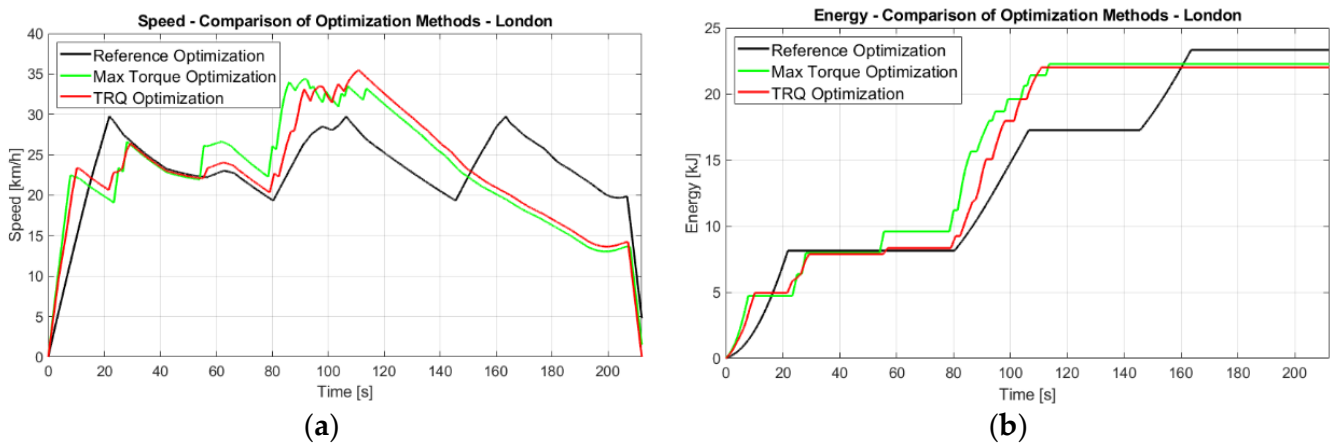


Figure 11. Track optimization results for London Track; (a) speed profile; (b) energy consumption.

Table 4. Optimization parameters and results for London Track.

Optimization Case	Reference	Max Torque	TRQ
Initial Population (N_{pop})	200	1380	1380
Function Variable (N_{var})	4	138	138
Best result	23,326 J	22,268 J	22,017 J
Generation	75	160	157
Function count	3578	219,776	215,681
Energy Saving	-	4.54%	5.61%

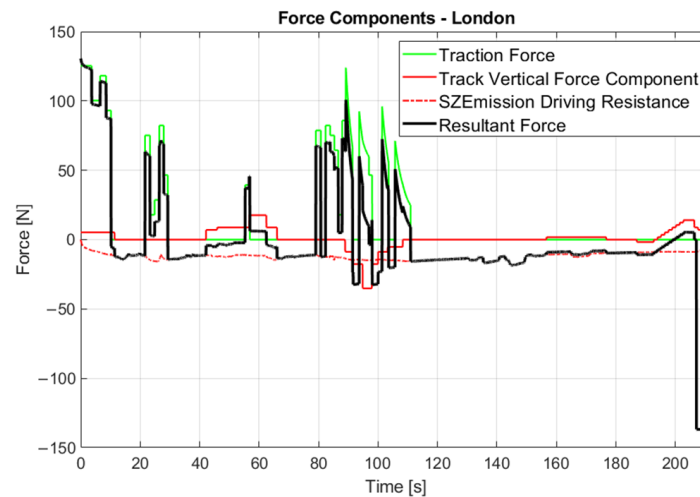


Figure 12. The resulting force components of the driving strategy on the London Track by TRQ optimization.

The vertical force component of the track is the most crucial local resistance, which influences the timing of the accelerations. The driving resistance is vehicle speed dependent, but it can be considered a continuous load due to the small aerodynamic drag even at higher speeds.

The Uni Track functions as a proving ground in ZalaZone for an autonomous and urban vehicle for university research. The track length is 576 m, which is much shorter than the London Track, and has a higher elevation difference. The reference optimization manages the speed between 15 km/h and 30 km/h with just one intermediate acceleration. The Max Torque optimization operates with three intermediate accelerations, but these prove to be too intensive, which is found by TRQ optimization according to Figure 13a.

The moderate acceleration applied by this method resulted in more accurate speed control and less energy consumption, which is visualized in Figure 13b.

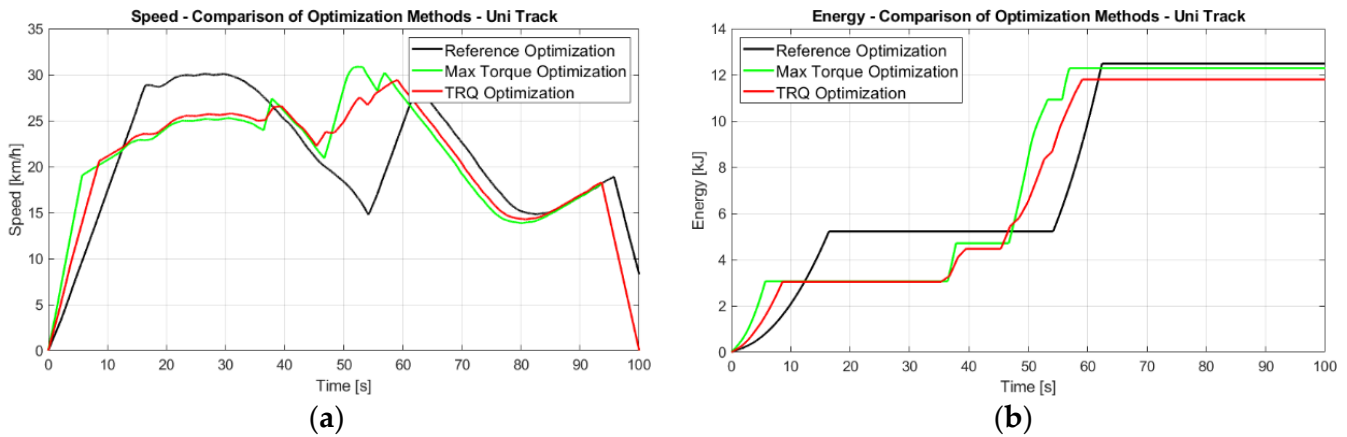


Figure 13. Track optimization results for Uni Track; (a) speed profile; (b) energy consumption.

The optimization parameters and results are illustrated in Table 5. The best result of the Max Torque method is just slightly more favorable than the reference, while the TRQ optimization results in a 5.5% improvement compared to the reference optimization.

Table 5. Optimization parameters and results for Uni Track.

Optimization Case	Reference	Max Torque	TRQ
N_{pop}	200	580	580
N_{var}	4	58	58
Best result	12,485 J	12,285 J	11,798 J
Generation	67	88	83
Function count	6470	51,186	48,311
Energy Saving	-	1.6%	5.5%

The trend of the force components in Figure 14 is comparable to the previous graph in Figure 12. The track vertical force component can almost double the total other vehicle driving resistance, marking the importance of track related optimization.

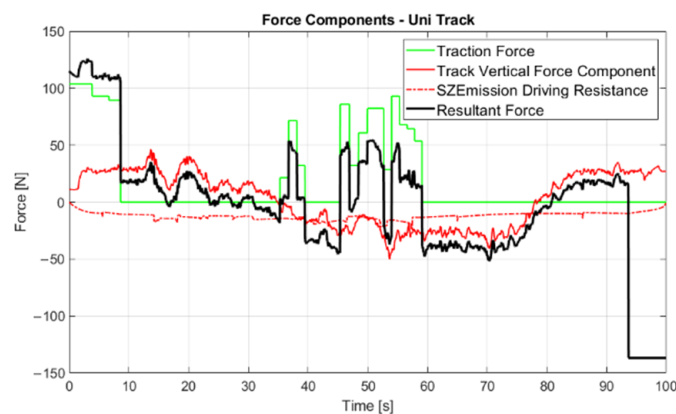


Figure 14. The resultant force components of the driving strategy on the London Track by TRQ optimization.

The resultant velocity profile and torque reference can be displayed on the main screen of the vehicle as a driving pattern for the driver. The driving profile can be replicated by following the displayed pattern. Based on the acceleration demand of the vehicle,

LED lights are blinking, which also supports the driver. Naturally, the human driver is going to differ from the described optimal pattern to some extent. During the autonomous operation of the vehicle, the control system could exactly follow the predetermined torque reference according to the GPS coordinates and vehicle speed. Test field measurements are needed to define the exact driving error of the human driver and autonomous operation. This measurement is going to be considered in the validation of the presented optimization results.

7. Conclusions

Altogether, three optimization methods were elaborated using the described vehicle model for the two investigated tracks. The reference optimization was defined in the literature, which sets vehicle speed and torque limits for the vehicle operation during the lap. The result does not consider the track characteristics, because the extent and timing of acceleration is fixed. The proposed Max Torque method evaluates the traction force demand throughout the whole track and determines the places of acceleration. The extent of acceleration is not discussed, and the available maximal torque is used. To further improve the result of this method, the TRQ optimization was applied, where the previously defined places of acceleration were monitored. The TRQ optimization builds on the Max Torque method by using its result to assign proper torque values to the places of acceleration. The TRQ optimization was unable to locate the correct timing and extent of acceleration at first, therefore the Max Torque method serves as an intermediate step. The application of the described optimization framework resulted in 5.61% and 5.5% energy savings compared to the reference method in the respective analyzed tracks. The results of the optimization methods are summarized in Figure 15.

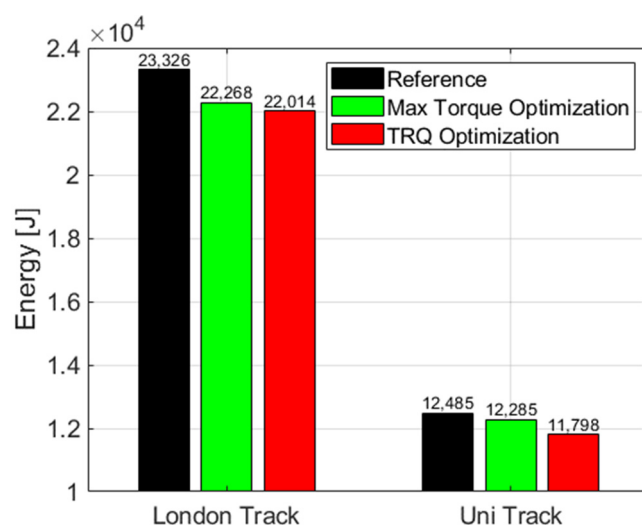


Figure 15. The energy demand of the studied track optimization methods.

Energy recuperation is not included in the proposed vehicle model and optimization. The process of regenerative braking can be similarly optimized, such as the acceleration if the powertrain model is extended to the regenerative operation. It is important to note that the theoretical optimization of the energy recuperation process does not mean the efficient recharging of the battery. The SOC state of the battery is not measured by the regulations of SEM, therefore the DC current is not limited. The effect of the wind is not considered in the vehicle model, while it is the most remarkable external factor of the driving strategy optimization. The external factors cause a problem for every investigated optimization method, therefore the application of neural networks could provide improvement in that field in the future. The application of driving strategy optimization will be essential to further reduce the CO₂ emission in the transportation and could have an even higher impact on the autonomous vehicles.

Author Contributions: Conceptualization, methodology, validation, formal analysis, and visualization Z.P. and P.K.; writing—draft preparation Z.P.; supervision, project administration, funding acquisition F.S. and F.F. All authors have read and agreed to the published version of the manuscript.

Funding: Project no. TKP2021-NKTA-48 has been implemented with the support provided by the Ministry of Innovation and Technology of Hungary from the National Research, Development and Innovation Fund, financed under the TKP2021-NKTA funding scheme.

Institutional Review Board Statement: Not applicable.

Informed Consent Statement: Not applicable.

Data Availability Statement: Not applicable.

Acknowledgments: Members of the SZEnergy Team (<https://szenergy.hu/>) provided internal telemetry data, images, and support during the field test, which the authors gratefully acknowledge.

Conflicts of Interest: The authors declare no conflict of interest.

References

1. IEA. *Global EV Outlook 2020*; IEA: Paris, France, 2020; Available online: <https://www.iea.org/reports/global-ev-outlook-2020> (accessed on 25 February 2022).
2. Hoekstra, A. The Underestimated Potential of Battery Electric Vehicles to Reduce Emissions. *Joule* **2019**, *3*, 1412–1414. [[CrossRef](#)]
3. Dominković, D.F.; Bačeković, I.; Pedersen, A.S.; Krajačić, G. The future of transportation in sustainable energy systems: Opportunities and barriers in a clean energy transition. *Renew. Sustain. Energy Rev.* **2018**, *82*, 1823–1838. [[CrossRef](#)]
4. Palencia, J.C.G.; Furubayashi, T.; Nakata, T. Energy use and CO₂ emissions reduction potential in passenger car fleet using zero emission vehicles and lightweight materials. *Energy* **2012**, *48*, 548–565. [[CrossRef](#)]
5. Egede, P. Electric Vehicles, Lightweight Design and Environmental Impacts. In *Environmental Assessment of Lightweight Electric Vehicles*; Egede, P., Ed.; Springer International Publishing: Cham, Switzerland, 2017; pp. 9–40. ISBN 978-3-319-40277-2.
6. Tóth, Á.; Szigeti, C.; Suta, A. Carbon Accounting Measurement with Digital Non-Financial Corporate Reporting and a Comparison to European Automotive Companies Statements. *Energies* **2021**, *14*, 5607. [[CrossRef](#)]
7. Shell Eco-Marathon. Shell Eco-Marathon 2022 Official Rules Chapter 1. 2022. Available online: <https://www.makethefuture.shell/en-gb/shell-eco-marathon/global-rules> (accessed on 25 February 2022).
8. Bingham, C.; Walsh, C.; Carroll, S. Impact of driving characteristics on electric vehicle energy consumption and range. *IET Intell. Transp. Syst.* **2012**, *6*, 29–35. [[CrossRef](#)]
9. Sciarretta, A.; De Nunzio, G.; Ojeda, L.L. Optimal Ecodriving Control: Energy-Efficient Driving of Road Vehicles as an Optimal Control Problem. *IEEE Control Syst.* **2015**, *35*, 71–90. [[CrossRef](#)]
10. Targosz, M.; Skarka, W.; Przystałka, P. Model-Based Optimization of Velocity Strategy for Lightweight Electric Racing Cars. *J. Adv. Transp.* **2018**, *2018*, 3614025. [[CrossRef](#)]
11. Sawulski, J.; Ławryńczuk, M. Optimization of control strategy for a low fuel consumption vehicle engine. *Inf. Sci.* **2019**, *493*, 192–216. [[CrossRef](#)]
12. Olivier, J.-C.; Wasselynck, G.; Chevalier, S.; Auvity, B.; Josset, C.; Trichet, D.; Squadrito, G.; Bernard, N. Multiphysics modeling and optimization of the driving strategy of a light duty fuel cell vehicle. *Int. J. Hydrog. Energy* **2017**, *42*, 26943–26955. [[CrossRef](#)]
13. Carello, M.; Bertipaglia, A.; Messina, A.; Airale, A.G.; Sisca, L. *Modeling and Optimization of the Consumption of a Three-Wheeled Vehicle*. SAE Technical Papers. 2019, pp. 1–9. Available online: <https://www.sae.org/publications/technical-papers/content/2019-01-0164/> (accessed on 6 April 2022).
14. Carmeli, M.S.; Castelli-Dezza, F.; Galmarini, G.; Mastinu, G.; Mauri, M. A Urban Vehicle with Very Low Fuel Consumption: Realization, analysis and optimization. In Proceedings of the 2014 9th International Conference on Ecological Vehicles and Renewable Energies, EVER 2014, Monte Carlo, Monaco, 25–27 March 2014; IEEE: Monte Carlo, Monaco, 2014; pp. 5–10.
15. Stabile, P.; Ballo, F.; Mastinu, G.; Gobbi, M. An Ultra-Efficient Lightweight Electric Vehicle—Power Demand Analysis to Enable Lightweight Construction. *Energies* **2021**, *14*, 766. [[CrossRef](#)]
16. Pusztai, Z.; Korös, P.; Friedler, F. Vehicle Model for Driving Strategy Optimization of Energy Efficient Lightweight Vehicle. *Chem. Eng. Trans.* **2021**, *88*, 385–390.
17. Pusztai, Z.; Körös, P.; Szauter, F.; Friedler, F. Hybrid Driving Strategy Optimization Using Cognitive Infocommunications. In Proceedings of the 12th IEEE International Conference on Cognitive Infocommunications (CogInfoCom), Győr, Hungary, 23–25 September 2021; pp. 435–440, ISBN 978-1-6654-2494-3.
18. Padilla, G.; Pelosi, C.; Beckers, C.; Donkers, M. Eco-Driving for Energy Efficient Cornering of Electric Vehicles in Urban Scenarios. *IFAC-PapersOnLine* **2020**, *53*, 13816–13821. [[CrossRef](#)]
19. Vaz, W.S.; Nandi, A.K.; Koylu, U.O. A Multiobjective Approach to Find Optimal Electric-Vehicle Acceleration: Simultaneous Minimization of Acceleration Duration and Energy Consumption. *IEEE Trans. Veh. Technol.* **2016**, *65*, 4633–4644. [[CrossRef](#)]
20. Albadr, M.A.; Tiun, S.; Ayob, M.; Al-Dhief, F. Genetic Algorithm Based on Natural Selection Theory for Optimization Problems. *Symmetry* **2020**, *12*, 1758. [[CrossRef](#)]

21. Watanabe, S.; Sato, Y.; Koseki, T.; Mizuma, T.; Tanaka, R.; Miyaji, Y.; Isobe, E. Verification of Optimized Energy-Saving Train Scheduling Utilizing Automatic Train Operation System. *IEEJ J. Ind. Appl.* **2020**, *9*, 193–200. [[CrossRef](#)]
22. Höschel, K.; Lakshminarayanan, V. Genetic algorithms for lens design: A review. *J. Opt.* **2018**, *48*, 134–144. [[CrossRef](#)]